Bactericidal Effect of Zero-Valent Iron Nanoparticles on *Escherichia coli*

Changha Lee[†], **Jee Yeon Kim**[‡], **Won Il Lee**[‡], **Kara L. Nelson**[†], **Jeyong Yoon**[*,‡], and **David L. Sedlak**[*,†]

[†]*Department of Civil and Environmental Engineering, 657 Davis Hall, University of California, Berkeley, California 94720*

[‡]*School of Chemical and Biological Engineering, College of Engineering, Seoul National University, San 56-1, Sillim-dong, Gwanak-gu, Seoul 151-742, Korea*

Abstract

Zero-valent iron nanoparticles (nano-Fe^0) in aqueous solution rapidly inactivated *Escherichia coli* (*E. coli*). A strong bactericidal effect of nano-Fe^0 was found under deaerated conditions, with a linear correlation between log inactivation and nano-Fe^0 dose (0.82 log inactivation / mg/L nano-$Fe^0 \cdot$ hr). The inactivation of *E. coli* under air saturation required much higher nano-Fe^0 doses due to the corrosion and surface oxidation of nano-Fe^0 by dissolved oxygen. Significant physical disruption of the cell membranes was observed in *E. coli* exposed to nano-Fe^0, which may have caused the inactivation, or enhanced the biocidal effects of dissolved iron. The reaction of Fe(II) with intracellular oxygen or hydrogen peroxide also may have induced oxidative stress by producing reactive oxygen species. The bactericidal effect of nano-Fe^0 was a unique property of nano-Fe^0, which was not observed in other types of iron-based compounds.

Introduction

With recent advances in nanotechnology, various types of metal and metal oxide nanoparticles with antimicrobial (microbiocidal or growth-inhibiting) activity have been synthesized (1–9). These compounds have a wide range of potential applications in biomedical fields (1,2), in textile fabrics (3), and in water treatment as disinfectants (4) or antibiofilm agents (5). Metal nanoparticles containing magnesium oxide (6), copper (7), and silver (1–5,8–10) exhibit antimicrobial properties. Among them, silver-based nanoparticles have been most intensively investigated due to their strong antimicrobial activity and the relatively low toxicity to humans (11). While the mechanism of antimicrobial activities of these metal nanocompounds is still not clearly understood, a variety of hypotheses have been proposed, including physical disruption of cell structures (6), disturbances of permeability and respiration (8–10), and damage of DNA or enzymatic proteins by metal ions released from the nanoparticles (8,10, 12).

Zero-valent iron (Fe^0) has been used in permeable reactive barriers for remediation of groundwater contaminated with halogenated solvents (13,14). Direct electron transfer from metallic iron to contaminants has been recognized as the main pathway of contaminant transformation by Fe^0 in the subsurface. In the presence of oxygen, the contaminants can also be oxidized by hydroxyl radical and other oxidants generated during the corrosion process of

---
*Address correspondence to either author. Phone: +82-2-880-8927 (J. Yoon); +1-510-643-0256 (D. L. Sedlak), Fax.: +82-2-876-8911 (J. Yoon); +1-510-642-7483 (D. L. Sedlak), E-mail: jeyong@snu.ac.kr (J. Yoon); sedlak@ce.berkeley.edu (D. L. Sedlak).

Fe^0 (15). Zero-valent iron nanoparticles (nano-Fe^0) recently have been shown as an effective alternative to granular Fe^0 (16,17). The advantages of nano-Fe^0 over microscale granular Fe^0 include its improved mobility and increased reactivity due to its higher surface area (16–18).

Despite increasing interest in the antimicrobial activity of metal nanoparticles and the widespread use of nano-Fe^0 for environmental remediation, little is known about the antimicrobial activity of nano-Fe^0. Previous investigators have reported on inactivation of bacteriophages by other types of iron-based compounds such as iron oxide-coated sands (19) or microscale iron powder (20). However, the biocidal activity required relatively high doses (several g/L) or long treatment times (for days or weeks), indicating that their biocidal activities are negligible compared to that of nano-Fe^0 demonstrated in this study. This study describes a strong bactericidal effect of nano-Fe^0 on *Escherichia coli* (*E. coli*). This bactericidal effect was found to be a size-related and element-specific property of nano-Fe^0. A substantial increase in antimicrobial activity was observed in the absence of oxygen.

Materials and Methods

Reagents and Synthesis of Nano-Fe^0

All chemicals for experiments were of reagent grade and used without further purification. All solutions were prepared in distilled and deionized water (Barnstead NANO Pure) saturated with air ($[O_2]_0 = 0.25$ mM). Nano-Fe^0 was synthesized by aqueous-phase reduction of ferrous sulfate using sodium borohydride as described previously (17. 21). Ferrous sulfate solution (2.0 g $FeSO_4 \cdot 7H_2O$ in 200 ml) in N_2 saturated water was reduced by the dropwise addition of sodium borohydride solution (0.4 g of $NaBH_4$ in 50 mL) using a separatory funnel at the rate of 1 ~ 2 drops per second. The suspension of nano-Fe^0 produced by this procedure was centrifuged for 4 minutes at 4000 rpm and washed with N_2 saturated 10^{-4} N HCl solution three times. Nano-Fe^0 produced by this method usually contains about 4 – 5 wt% of boron (22,23). Additional details of the nano-Fe^0 synthesis procedure are described in Supporting Information, S1.

Figure 1a shows the morphology of nano-Fe^0, measured with a JEM-2000XII (JEOL Ltd.) transmission electron microscope (TEM) at 120 kV. In agreement with previous studies (17), nano-Fe^0 forms chain-shaped aggregates of spherical single nanoparticles ranging over 10 – 80 nm in diameter (average diameter ≈ 35 nm). The N_2-BET surface area was determined as 34.5 m^2/g.

Culture and Analysis of *E. coli*

E. coli (ATCC strain 8739) was inoculated in 50 mL of Tryptic Soy Broth (Difco Co., Detroit, Mich.) medium and grown at 37°C for 18 h. The bacteria were harvested by centrifugation at $1000 \times g$ for 10 min and washed twice with 50 mL of 150 mM phosphate buffered saline (PBS, pH 7.2). The stock suspension of *E. coli* was prepared by resuspending the final pellets in 50 mL of 150 mM PBS solution. The population of *E. coli* in the stock suspension ranged over $1 \times 10^9 \sim 2 \times 10^9$ CFU (Colony Forming Unit) / mL. The number of cells was determined by the spread plate method, in which *E. coli* cells were plated on nutrient agar, incubated at 37°C for 24 h, and the number of colonies counted.

Inactivation Experiments

The inactivation experiments were performed at room temperature (21 ± 0.5°C) using a 50 mL *E. coli* cell suspension of $1 \times 10^6 \sim 2 \times 10^6$ CFU/mL, prepared by diluting *E. coli* stock suspension in 2 mM carbonate buffer solution (pH = 8.0). The concentrations of nano-Fe^0 employed in this study ranged from 1.2 to 110 mg/L. The experiments under air saturation

were performed with the reactor sealed (closed air-saturated) or exposed to the atmosphere (open air-saturated). For deaeration of the reaction solution, the reactor was sealed with a rubber septum, and ultra-pure N_2 gas was bubbled with a needle-type diffuser for 10 min prior to initiation of the experiment. The inactivation experiments were initiated by adding an aliquot of freshly prepared nano-Fe^0 stock suspension (9.0 g/L aqueous suspension). The *E. coli* suspension was mixed by continuous stirring during the entire experiment. A slight pH increase (< 0.2) was observed after the reaction under air saturation. Samples of 1 mL were withdrawn at predetermined timed intervals, and quickly diluted 1/100, 1/1000, and 1/10000 with air-saturated water. The dilution in oxygenated water quenched the further inactivation of *E. coli* by lowering the concentration of nano-Fe^0 and oxidizing the iron particles. Triplicate plates were used for counting viable cells from each diluted suspension. Most of the experiments were performed in triplicate; the average values and the standard deviations are presented.

Transmission Electron Microscopy Analysis of *E. coli* cells

The TEM specimens of *E. coli* cells were prepared by the following procedures. The native and treated cells were quickly fixed in 2% glutaraldehyde and 0.05 M sodium cacodylate buffer (pH 7.2), followed by washing three times with 0.05 M sodium cacodylate buffer and postfixing with 1% osmium tetroxide in 0.05 M sodium cacodylate buffer for 2 h. After fixation, the samples were concentrated by centrifugation at $2500 \times g$ for 2 min, and washed twice with distilled water. The concentrated cells were dehydrated with sequential treatment with 30, 50, 70, 80, 90 and 100% ethanol for 10 min. The cells were then infiltrated and embedded in Spurr's resin with propylene oxide (treatment with 3:1, 2:1, 1:1, 1:2, and 1:3 of propylene oxide:Spurr's resin mixtures for 30 min each, and 100% Spurr's resin for 25 hr). The samples, filled with Spurr's resin, were cured overnight at 70°C to form sample blocks. The polymerized blocks were sectioned using an ultramicrotome (MT-X, RMC), and the thin sections were stained in 2% uranyl acetate and Reynold's lead citrate, and examined by TEM at 80 kV accelerating potential.

Results and Discussion

Inactivation of *E. coli* by Nano-Fe^0 under Air Saturation and Deaeration

The *E. coli* inactivation was expressed as $\log(N/N_0)$, where N and N_0 are the remaining and initial numbers of viable *E. coli* cells (CFU/mL), respectively. In control experiments, the number of viable *E. coli* cells varied by less than 0.1 log units ($\approx$ 20%) after 1 hr in 2 mM carbonate buffer solution (pH = 8.0) under both air-saturated and deaerated conditions. The inactivation of *E. coli* in the solution containing 1 mM sodium tetraborate ($Na_2B_4O_7$) or oxidized products of 1 mM sodium borohydride also was negligible afer 1 hr (<0.1 log units), indicating that boron-containing compounds, which may be released from nano-Fe^0, do not cause the *E. coli* inactivation.

A strong bactericidal effect of nano-Fe^0 was found in the absence of oxygen, with a direct relationship between *E. coli* inactivation and nano-Fe^0 dose, whereas nano-Fe^0 under air saturation showed limited inactivation (Figure 2). Ninety mg/L nano-Fe^0 in an air-saturated suspension resulted in 2.6 and 3.6 log inactivation of *E. coli* for 60 min in the open and closed reactor systems, respectively (Figure 2a). The inactivation curves under air saturation exhibited a decrease in inactivation rate with time, whereas the deaerated condition showed a much higher inactivation rate, and no diminution in activity with time: 3.4 log inactivation was achieved after 10 min contact with 9 mg/L nano-Fe^0. The high biocidal activity of nano-Fe^0 to *E. coli* in the absence of oxygen, the absence of an effect of adding a hydroxyl radical ($^\bullet$OH) scavenger (*tert*-butyl alcohol) under air-saturated conditions indicate that the direct damage via $^\bullet$OH in bulk phase produced from oxygen-induced corrosion of nano-Fe^0 does not significantly contribute to *E. coli* inactivation.

The effect of nano-Fe^0 on log inactivation of *E. coli* after 1 hr of treatment was much greater under deaerated than under air-saturated (open and closed) conditions (Figure 2b). The dose-log inactivation curve under deaerated conditions was linear ($r^2 = 0.99$) with a slope of 0.82 (log inactivation / mg/L nano-Fe^0). Under air saturation, *E. coli* inactivation was much lower, with less than 1 log below doses of 60 mg/L nano-Fe^0. Substantial *E. coli* inactivation was only observed above 60 and 70 mg/L nano-Fe^0 doses in closed and open air-saturated systems, respectively. Under air-saturated closed conditions, the dissolved oxygen concentration decreased with increasing nano-Fe^0 dose (dashed line in Figure 2b; measured by the spectrophotometric Winkler method; 24). After the oxygen was depleted by nano-Fe^0 corrosion, the remaining unoxidized nano-Fe^0 appears to have been responsible for the enhanced inactivation.

Oxidation and Surface Passivation of Nano-Fe^0

The reduction of bactericidal activity of nano-Fe^0 in the presence of dissolved oxygen is most likely related to oxidation of nano-Fe^0 (also refer to experiments 2, 3 in Table 1). Oxidation of Fe^0 by oxygen leads to the formation of an iron oxide layer on the nano-Fe^0 surface (25). The activity of nano-Fe^0 under air saturation was affected by addition of Fe(III)-chelating agents (experiments 10, 11 in Table 1). Phosphate ion, which can form insoluble amorphous complexes with Fe(III) on the nano-Fe^0 surface, reduced the bactericidal activity of nano-Fe^0, whereas oxalate ion, which forms soluble Fe(III)-complexes, increased the biocidal activity by preventing the build-up of an iron oxide layer on the nanoparticle surface.

Further evidence that oxidation of nano-Fe^0 inhibited biocidal activity of nano-Fe^0 was obtained by measuring the rate at which nano-Fe^0 was oxidized by dissolved oxygen at low nano-Fe^0 doses, and by observing TEM images of oxidized nano-Fe^0. The color of nano-Fe^0 suspension changed from black to yellow as Fe(III) was produced under air-saturated conditions (Figure 1d). The aqueous suspension of nano-Fe^0 prior to exposure to oxygen showed a constant UV/visible absorbance over the entire wavelength range without any characteristic peaks, and was stable under deaerated conditions. Under air-saturated conditions, a broad UV/visible absorption band centered at around 390 nm evolved as the oxidation of nano-Fe^0 proceeded. The increase of UV absorbance at 390 nm occurred rapidly, and was complete in approximately 10 min. This rapid oxidation of nano-Fe^0 by dissolved oxygen significantly reduced the exposure of *E. coli* to unoxidized nano-Fe^0 under air-saturated conditions.

The exposures of unoxidized nano-Fe^0, ∫[nano-Fe^0]dt under air saturation were calculated from the time-dependent variation in the UV/visible absorption spectrum of nano-Fe^0 suspension (Figure 3a). Fort each set of experimental conditions, the concentration of unoxidized nano-Fe^0 was determined at each time from UV absorbance at 390 nm. Then, the cumulative exposure to unoxidized nano-Fe^0 (∫[nano-Fe^0]dt, mg·s/L) was calculated by integrating [nano-Fe^0](t) with respect to time. Details for the calculation are provided in Supporting Information, S2. In air-saturated experiments with 18 ~ 54 mg/L nano-Fe^0 (insufficient doses for the complete depletion of dissolved oxygen), the exposures of *E. coli* to unoxidized nano-Fe^0 were calculated to be $(1.1 \sim 9.0) \times 10^3$ mg·s/L (i.e., 0.3 ~ 2.5 mg/L·hr). These initial phases of nano-Fe^0 exposure under air saturation appear to fit well with those of the *E. coli* inactivation curves in Figure 2b. The plots of *E. coli* log inactivation against the ∫[nano-Fe^0]dt values show linearity (Figure 3b), indicating that the observed inactivation curves were effectively explained by assuming that only unoxidized nano-Fe^0 inactivates *E. coli*. The lower slopes under air saturation than that under deaeration appear to be due to the reduced reactivity of unoxidized nano-Fe^0 in the presence of oxidized nano-Fe^0. The iron precipitates from oxidation of nano-Fe^0 may deposit on the reactive surface of nano-Fe^0, and decrease its biocidal activity. This explanation was supported by the observation that the addition of 90 mg/L oxidized nano-

Fe^0 into 9 mg/L nano-Fe^0 under deaerated conditions decreased the *E. coli* inactivation from 3.4 to 2.0 log for 10 min contact time.

TEM images of nano-Fe^0 after exposure to air illustrate the effect of oxidation on the particle surface. Upon exposure to oxygen, nano-Fe^0 particles are rapidly oxidized to produce iron precipitates (fibers) on the surface (Figure 1b), which are presumably a Fe(III) oxide-hydroxide. All of the nano-Fe^0 particles were converted to fibers after 60 min of oxidation (Figure 1c).

Inactivation of *E. coli* by Other Iron-Based Compounds

To gain insight into the mechanism of *E. coli* inactivation by nano-Fe^0, additional inactivation experiments were performed with several iron compounds (Table 1). No significant inactivation of *E. coli* was achieved after 1 hr treatment with 9 mg/L iron oxide (magnetite) nanoparticles (experiment 1 in Table 1) or 1 g/L microscale Fe^0 powder (experiment 4 in Table 1). 1 g Fe^0 powder had a BET surface area of 0.26 m^2, which is similar to that of 9 mg/L nano-Fe^0 (9 mg/L × 31.4 m^2/g = 0.28 m^2/L) (experiment 8 in Table 1). These results suggest that the biocidal effect of nano-Fe^0 originates from both a size-related physical property of nanoparticles and a chemical interaction of elemental iron with *E. coli*. Although You et al. (20) recently reported 1 ~ 2 log removals of bacteriophages, φX174 and MS-2 after 1 hr treatment with Fe^0 powder, the activity is not comparable to that of nano-Fe^0. They used a high concentration of iron powder (4 g/L × 1.67 m^2/g = 6.68 m^2/L), which has more than 20 times higher surface area than the conditions employed in this study. Moreover, the observed removal includes not only potential inactivation of viruses but also their irreversible adsorption on the iron surface.

Significant inactivation of *E. coli* by ferrous (Fe[II]) ion under deaerated conditions (experiment 7 in Table 1) suggested that Fe(II) ion released from metallic iron can contribute to the bactericidal activity of nano-Fe^0. In contrast, ferric (Fe[III]) ion did not inactivate *E. coli* regardless of oxygen concentration (experiment 5 in Table 1), possibly due to the low solubility of Fe(III) ion in neutral aqueous solution. The absence of bactericidal effect of Fe(II) ion in the air-saturated solution (experiment 6 in Table 1) is attributed to the rapid oxidation of Fe(II) into Fe(III) by dissolved oxygen in the neutral pH region ($k_{Fe(II)+O2}$ at pH 8.0 = 170 M^{-1} s^{-1}; $\tau_{1/2, Fe(II)}$ = 16 s under air saturation; 26). The concentration of Fe(II) ion released from 9 mg/L nano-Fe^0 under deaerated conditions was less than 10 μM as determined using the 1,10-phenanthroline method (27). 10 μM Fe(II) ion under deaerated conditions resulted in only 0.9 log inactivation of *E. coli* after 1 hr (Figure 2a). However, the exposure of *E. coli* to Fe(II) may be much higher in nano-Fe^0 suspension because the nanoparticle surface have an affinity for the cells.

Morphological Changes in *E. coli* cells and Possible Inactivation Mechanisms

The TEM images of the *E. coli* cells treated with Fe(II) ion under deaerated conditions (Figure 4c & 4d) provide insight into the mechanism of inactivation. The treated cells contain dark spots along the inside cell wall and within the cytoplasm. These specks are likely Fe(III) oxide particles formed via oxidation of Fe(II) ion after it passed into the cells. The pretreatment steps for TEM analysis after sample collection possibly allowed the oxygen exposure to *E. coli* cells, but it is unclear in which step the oxidation of Fe(II) occurred. Despite these limitations, it is evident that the oxidized iron oxides are located inside the cytoplasmic membrane (Figure 4d), implying that Fe(II) ions entered the cytoplasm of *E. coli* after disruption of Fe(II) ion regulating system (28,29). Although the mechanism for the bactericidal action of Fe(II) ion is not fully understood, the presence of Fe(II) likely induced oxidative stress by producing reactive oxygen species through the Fenton reaction (30), which could occur through contact with oxygen after the inactivation experiment or intracellular oxygen or hydrogen peroxide

present when the cells were introduced to the deaerated reactor. It is unclear whether Fe(II) ions binding to DNA or specific proteins may directly prevent cell replication or hinder enzymatic function.

TEM images of *E. coli* cells treated with nano-Fe^0 (Figure 4e & 4f) exhibit different morphologies from the Fe(II) ion-treated cells. Significant disruption of the cell membranes (Figure 4f) and the subsequent leakage of the intracellular contents were observed (refer to Supplementary Information, S4 for more TEM images). The chemical interactions between the reactive surfaces of nano-Fe^0 and *E. coli* cells are primarily responsible for the disruption of cell membranes. Iron is a strong reductant ($E_H^0(Fe^{2+}/Fe^0) = -0.447$ V; 31) and it is possible that it induced reductive decompose of functional groups in the proteins and lipopolysaccharides of the outer membranes. Alternatively nano-Fe^0 may have been oxidized by intracellular oxygen, leading to oxidative damages via the Fenton reaction. It appears that nano-Fe^0 penetrates into the cells through the vulnerable membranes after the chemical disruption, causing more serious physical damages. Small nanoparticles (< 10 nm) of the chemically-inert compounds such as magnesium oxide (6) and zinc oxide (32) have shown to penetrate into *E. coli* cells without leading to as much disruption of cell walls as nano-Fe^0.

The serious physical disruption of cell integrity caused by nano-Fe^0 may have resulted in inactivation and it also may have enhanced the biocidal effects by chemical interactions of nano-Fe^0 with *E. coli* cells. In spite of the different observed morphologies, it is possible that Fe(II) ion released from nano-Fe^0 contributes to the *E. coli* inactivation, because the physical damage to cell membranes can significantly decrease the lethal dose of Fe(II) ion by facilitating its transport into the cell. In addition, the reducing power of iron may disturb the enzymatic function of external membrane proteins of *E. coli* by direct electron transfer. However, the hypothesized mechanisms of inactivation discussed above have not been proven, and further investigations, including measurements of enzymatic function, are needed to better understand the mechanism of bactericidal action of nano-Fe^0.

Nano-Fe^0 as a Strong Bactericide

Nano-Fe^0 showed a strong bactericidal activity comparable to that of silver nanoparticles. The efficiencies of *E. coli* inactivation by nano-Ag^0 (0.30 & 0.41 log inactivation / (mg/L·hr); experiments 12 & 13 in Table 1) are between the values by nano-Fe^0 under air saturated (experiment 8) and deaerated conditions (experiment 9). Nano-Ag^0 showed a slightly higher activity under air saturation probably due to the oxygen-induced dissolution of silver ion (Ag^+). The strong bactericidal activity of nano-Fe^0 implies that nano-Fe^0 can serve as a cost-effective biocide for many of the applications in which silver is being used. However, the reduction of bactericidal activity of nano-Fe^0 by oxidative corrosion will limit its application. Alternatively, it may be possible to synthesize nanoparticles in forms that resist oxidation. Because the toxicity of engineered nanoparticles is one of the key uncertainties associated with widespread application of nanotechnology (33–35), oxidation of the nano-Fe^0 surface may be considered as a means of decreasing the toxicity of the nanoparticles.

Supplementary Material

Refer to Web version on PubMed Central for supplementary material.

Acknowledgements

Literature Cited

1. Alt V, Bechert T, Steinrcke P, Wagener M, Seidel P, Dingeldein E, Domann U, Schnettler R. An in vitro assessment of the antibacterial properties and cytotoxicity of nanoparticulate silver bone cement. Biomaterials 2004;25:4383–4391. [PubMed: 15046929]

2. Furno F, Morley KS, Wong B, Sharp BL, Arnold PL, Howdle SM, Bayston R, Brown PD, Winship PD, Reid H. Silver nanoparticles and polymeric medical devices: a new approach to prevention of infection? J Antimicrob Chemother 2004;54:1019–1024. [PubMed: 15537697]

3. Jeong SH, Yeo SY, Yi SC. The effect of filler particle size on the antibacterial properties of compounded polymer/silver fibers. J Mater Sci 2005;40:5407–5411.

4. Chou WL, Yu DG, Yang MC. The preparation and characterization of silver-loading cellulose acetate hollow fiber membrane for water treatment. Polym Adv Technol 2005;16:600–607.

5. Sambhy V, MacBride MM, Peterson BR, Sen A. Silver bromide nanoparticle/polymer composites: Dual action tunable antimicrobial materials. J Am Chem Soc 2006;128:9798–9808. [PubMed: 16866536]

6. Stoimenov PK, Klinger RL, Marchin GL, Klabunde KJ. Metal oxide nanoparticles as bactericidal agents. Langmuir 2002;18:6679–6686.

7. Hsiao MT, Chen SF, Shieh DB, Yeh CS. One-pot synthesis of hollow Au3Cu1 spherical-like and biomineral botallackite Cu-2(OH)(3)Cl flowerlike architectures exhibiting antimicrobial activity. J Phys Chem B 2006;110:205–210. [PubMed: 16471522]

8. Morones JR, Elechiguerra JL, Camacho A, Holt K, Kouri JB, Ramírez JT, Yacaman MJ. The bactericidal effect of silver nanoparticles. Nanotechnology 2005;16:2346–2353.

9. Sondi I, Salopek-Sondi B. Silver nanoparticles as antimicrobial agent: a case study on E-coli as a model for Gram-negative bacteria. J Colloid Interf Sci 2004;275:177–182.

10. Panáček A, Kvítek L, Prucek R, Kolář M, Večeřová R, Pizúrová N, Sharma VK, Nevěčná T, Zbořil R. Silver colloid nanoparticles: Synthesis, Characterization, and their antibacterial activity. J Phys Chem B 2006;110:16248–16253. [PubMed: 16913750]

11. Russell AD, Hugo WB. Antimicrobial activity and action of silver. Prog Med Chem 1994;31:351–370. [PubMed: 8029478]

12. Gogoi SK, Gopinath P, Paul A, Ramesh A, Ghosh SS, Chattopadhyay A. Green fluorescent protein-expressing Escherichia coli as a model system for investigating the antimicrobial activities of silver nanoparticles. Langmuir 2006;22:9322–9328. [PubMed: 17042548]

13. Matheson LJ, Tratnyek PG. Reductive dehalogenation of chlorinated methanes by iron metal. Environ Sci Technol 1994;28:2045–2053.

14. Farrell J, Kason M, Melitas N, Li T. Investigation of the long-term performance of zero-valent iron for reductive dechlorination of trichloroethylene. Environ Sci Technol 2000;34:514–521.

15. Joo SH, Feitz AJ, Sedlak DL, Waite TD. Quantification of the oxidizing capacity of nanoparticulate zero-valent iron. Environ Sci Technol 2005;39:1263–1268. [PubMed: 15787365]

16. Zhang WX. Nanoscale iron particles for environmental remediation: An overview. J Nanopart Res 2003;5:323–332.

17. Li L, Fan MH, Brown RC, Van Leeuwen JH, Wang JJ, Wang WH, Song YH, Zhang PY. Synthesis, properties, and environmental applications of nanoscale iron-based materials: A review. Crit Rev Environ Sci Technol 2006;36:405–431.

18. Hydutsky BW, Mack EJ, Beckerman BB, Skluzacek JM, Mallouk TE. Optimization of Nano- and Microiron Transport through Sand Columns Using Polyelectrolyte Mixtures. Environ Sci Technol 2007;41:6418–6424. [PubMed: 17948788]

19. Ryan JN, Harvey RW, Metge D, Elimelech M, Navigato T, Pieper AP. Field and laboratory investigations of inactivation of viruses (PRD1 and MS2) attached to iron oxide-coated quartz sand. Environ Sci Technol 2002;36:2403–2413. [PubMed: 12075796]

20. You Y, Han J, Chiu PC, Jin Y. Removal and inactivation of waterborne viruses using zerovalent iron. Environ Sci Technol 2005;39:9263–9269. [PubMed: 16382951]

21. Lowry GV, Johnson KM. Cogener-specific decomposition of dissolved PCBs by microscale and nanoscale zerovalent iron in a water/methanol solution. Environ Sci Technol 2004;38:5208–5216. [PubMed: 15506219]

22. Schrick B, Blough JL, Jones AD, Mallouk TE. Hydrodechlorination of trichloroethylene to hydrocarbons using bimetallic nickel-iron nanoparticles. Chem Mater 2002;14:5140–5147.

23. Liu Y, Choi H, Dionysiou D, Lowry GV. Trichloroethene hydrodechlorination in water by highly disordered monometallic nanoiron. Chem Mater 2005;17:5315–5322.

24. Labasque T, Chaumery C, Aminot A, Kergoat G. Spectrophotometric Winkler determination of dissolved oxygen: re-examination of critical factors and reliability. Mar Chem 2004;88:53–60.

25. Davenport AJ, Oblonsky LJ, Ryan MP, Toney MF. The structure of the passive film that forms on iron in aqueous environments. J Electrochem Soc 2000;147:2162–2173.

26. King DW, Lounsbury HA, Millero FJ. Rates and mechanism of Fe(II) oxidation at nanomolar total iron concentrations. Environ Sci Technol 1995;29:818–824.

27. Tamura H, Goto K, Yotsuyanagi T, Nagayama M. Spectrophotometric determination of iron(II) with 1, 10- phenanthroline in presence of large amounts of iron(III). Talanta 1974;21:314–318.

28. Kammler M, Schön C, Hantke K. Characterization of the ferrous iron uptake system of *Escherichia-Coli*. J Bacteriol 1993;175:6212–6219. [PubMed: 8407793]

29. Andrews SC, Robinson AK, Rodríguez-Quinones F. Bacterial iron homeostasis. Fems Microbiol Rev 2003;27:215–237. [PubMed: 12829269]

30. Touati D. Iron and oxidative stress in bacteria. Arch Biochem Biophys 2000;373:1–6. [PubMed: 10620317]

31. Bard, AJ.; Parsons, R.; Jordan, J. Standard potentials in aqueous solution. Marcel Dekker, Inc.; New York, Basel: 1985.

32. Brayner R, Ferrari-Iliou R, Brivois N, Djediat S, Benedetti MF, Fiévet F. Toxicological impact studies based on *Escherichia coli* bacteria in ultrafine ZnO nanoparticles colloidal medium. Nano Lett 2006;6:866–870. [PubMed: 16608300]

33. Nel A, Xia T, Mädler L, Li N. Toxic potential of materials at the nanolevel. Science 2006;311:622–627. [PubMed: 16456071]

34. Moore MN. Do nanoparticle present ecotoxicological risks for the health of the aquatic environment? Environ Int 2006;32:967–976. [PubMed: 16859745]

35. Hillie T, Hlophe M. Nanotechnology and the challenge of clean water. Nat Nanotechnol 2007;2:663–664. [PubMed: 18654395]
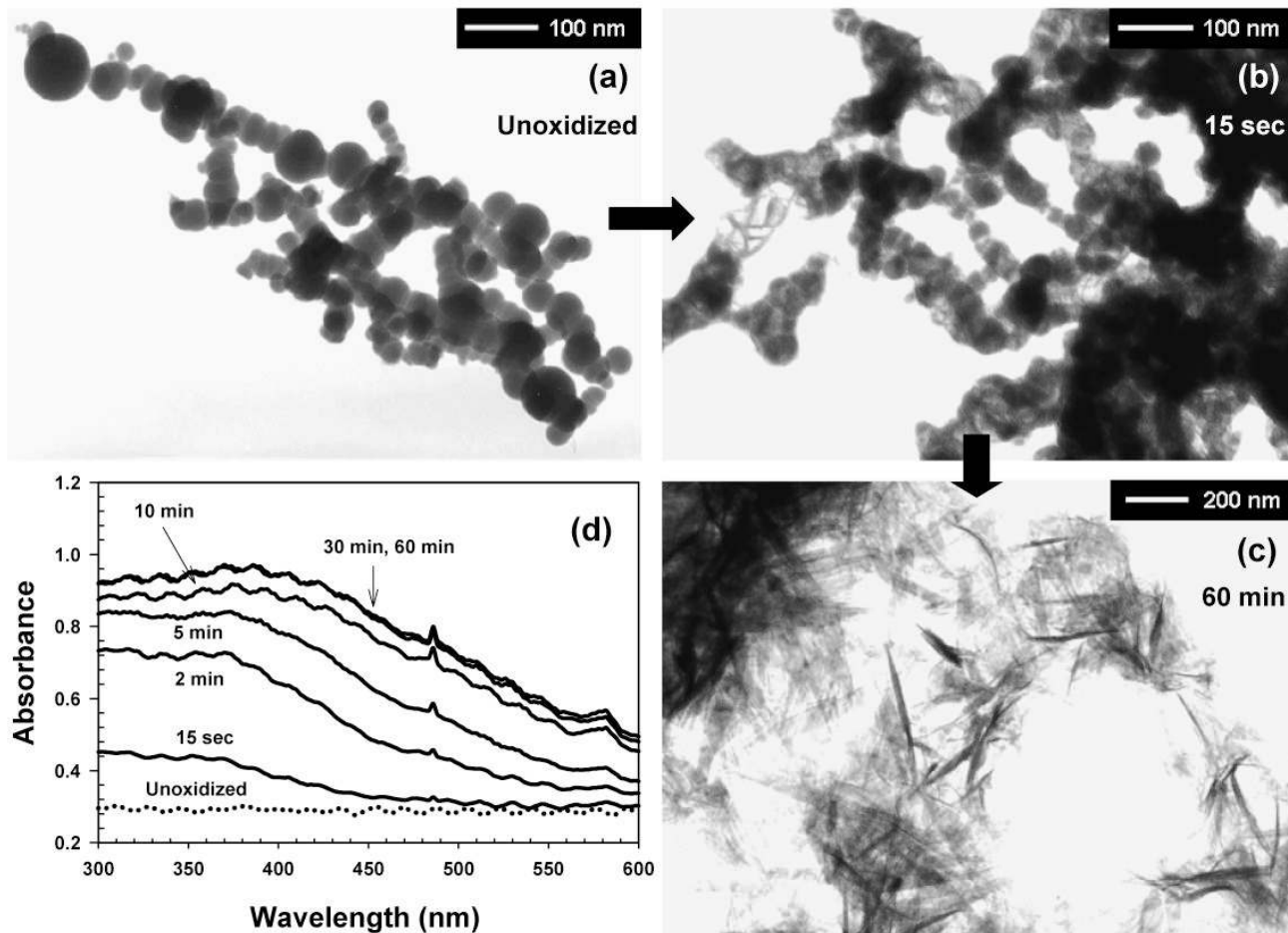
Figure 1.
TEM images of (a) unoxidized and (b, c) oxidized nano-Fe^0, and (d) variation in the UV-vis absorption spectrum of nano-Fe^0 solution under air saturation (open to air) ($pH_0 = 8.0$, 2 mM carbonate buffer, [nano-$Fe^0]_0 = 90$ mg/L).
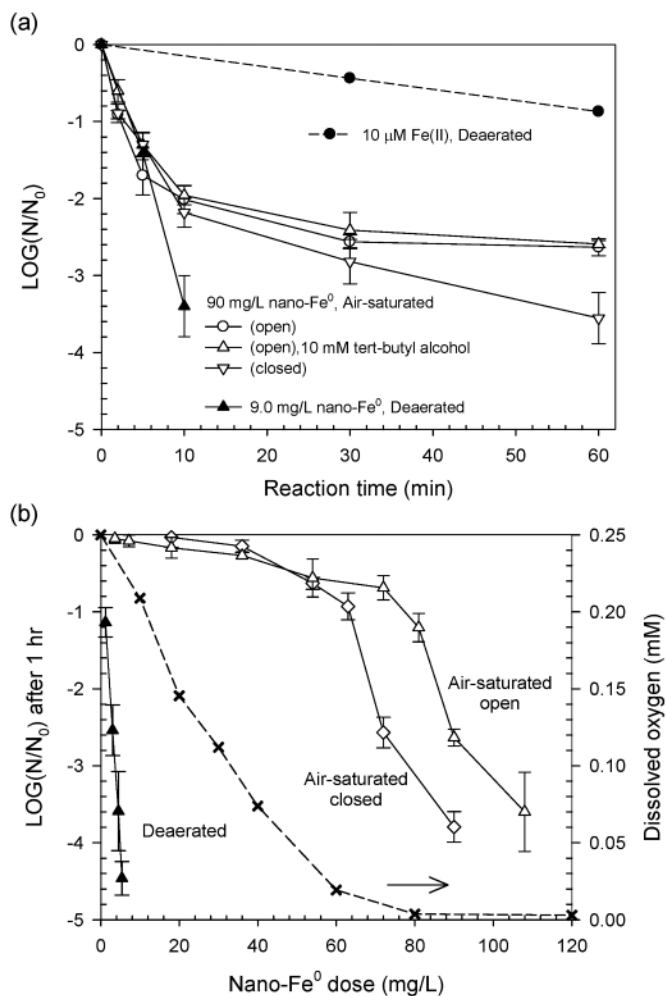
Figure 2.
Inactivation of *E. coli* by nano-Fe^0 as functions of (a) contact time and (b) nano-Fe^0 dose after 1 hr under air-saturated and deaerated conditions (pH$_0$ = 8.0, 2 mM carbonate buffer, The dashed line in Figure 2b indicates depletion of dissolved oxygen under air-saturated closed condition.)
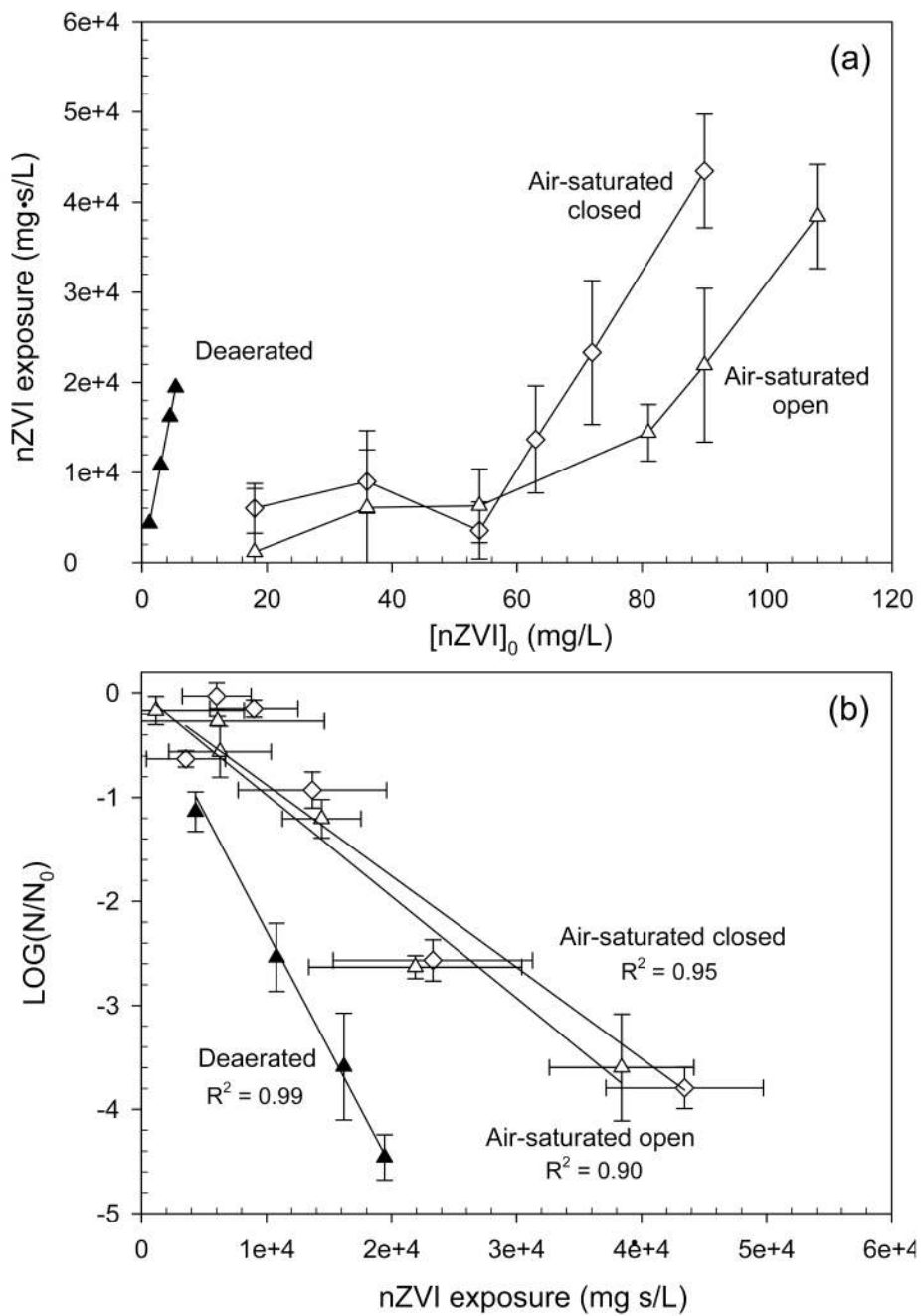
Figure 3.
(a) Nano-Fe^0 exposure for 1 hr contact time as a function of [nano-Fe^0]$_0$, and (b) plots of *E. coli* inactivation against nano-Fe^0 exposure (pH$_0$ = 8.0, 2 mM carbonate buffer).
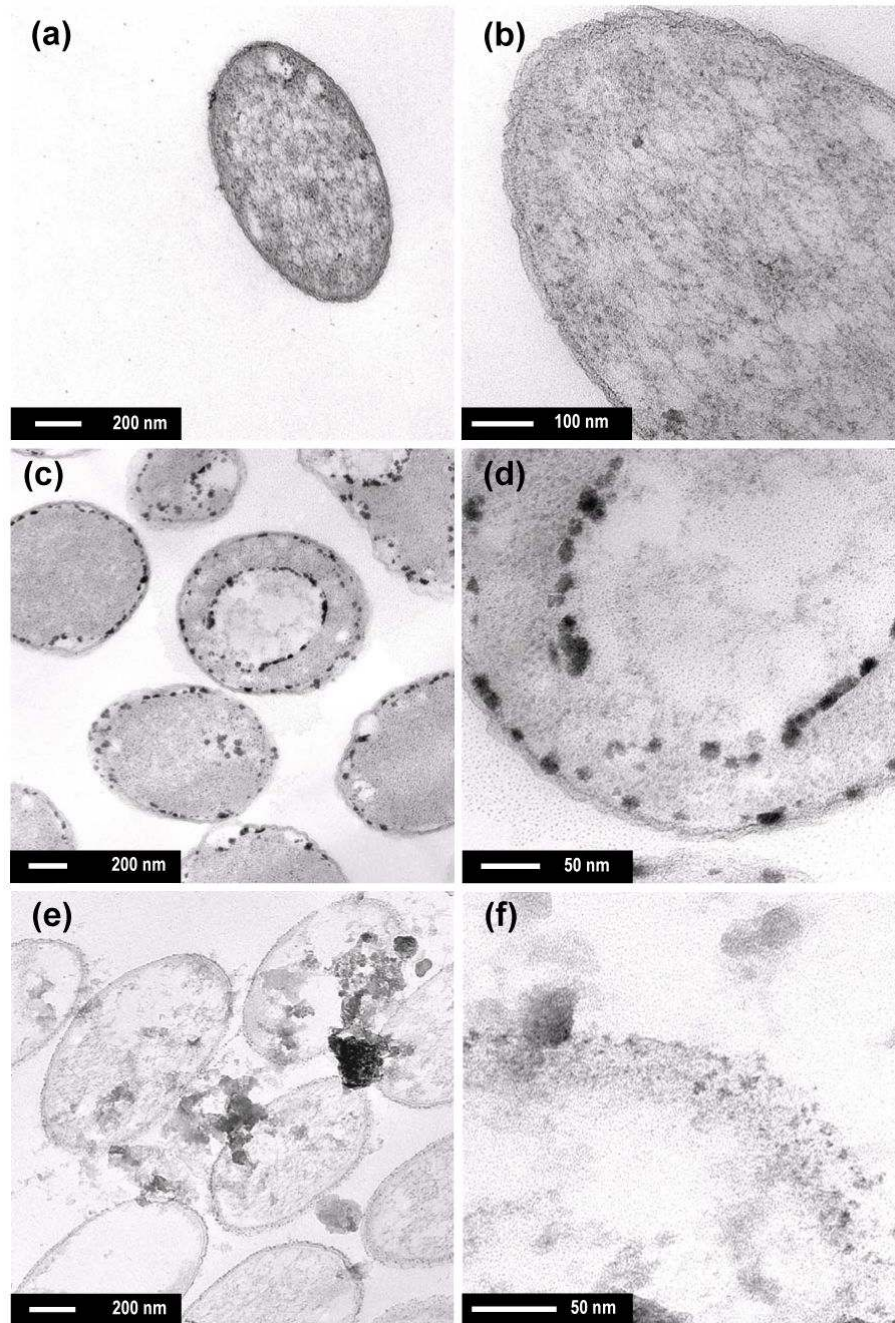
Figure 4.
TEM images of (a, b) native *E. coli* cells, and treated cells with (c, d) $FeSO_4$ and (e, f) nano-Fe^0 (> 3 log inactivation, [Fe(II)] = 0.1 mM for (c, d), [nano-Fe^0] = 10 mg/L for (e, f), pH = 8.0, 2 mM carbonate buffer, treatment time = 30 min under deaerated condition)

Table 1

Comparison of *E. coli* inactivation of several compounds in aqueous solution

No.	Compound	Conditions [c] (concentration, contact time, aeration etc.)	Log inactivation	Log inactivation / (mg/L·hr)
	Iron(II,III) oxide nanoparticle [a]			
1	Magnetite (Fe_3O_4), spherical < 50 nm, >60 m^2/g	9 mg/L, 1 hr, deaerated		
2	Oxidized nano-Fe^{0b}	9 mg/L, 1 hr, deaerated		
3		90 mg/L, 1 hr, air saturation	< 0.1	-
4	Iron (Fe^0) powder [a] < 10 μm, 0.26 m^2/g	1 g/L, 1 hr, deaerated		
5	Fe(III) ion ($FeCl_3$)	1 mM, 1 hr, air saturation and deaerated		
6	Fe(II) ion ($FeSO_4$)	0.1 mM, 1 hr, air saturation		
7		0.1 mM, 1 hr, deaerated	> 3	-
8		9 mg/L, 10 min, deaerated	3.4[d]	2.3
9	Nano-Fe^0 < 100 nm, 31.5 m^2/g	90 mg/L, 1 hr, air saturation	2.6[d]	0.029
10		90 mg/L, 1 hr, air saturation, 1 mM phosphate	1.3	0.014
11		45 mg/L, 1 hr, air saturation, 1 mM oxalate	3.1	0.069
12	Nano-Ag^{0e} 15 ~ 20 nm	10 mg/L, 1 hr, deaerated	3.0	0.30
13		10 mg/L, 1 hr, air saturation	4.1	0.41

[a] Obtained from Sigma-Aldrich Co.

[b] Oxidized for 2 hr under air saturation

[c] Unless otherwise specified: pH = 8.0 (carbonate buffer), T = 21±0.5°C, air saturation indicates open system to atmosphere

[d] From the data of Figure 2

[e] Prepared by photoreduction of silver ion in aqueous solution containing poly(ethylene oxide)–poly(propylene oxide)–poly(ethylene oxide) block copolymers (Supporting Information, S3)